CrossMark

Solution Processed p-Type Cu$_2$ZnSnS$_4$ Thin Films for Absorber Layer

G. Genifer Silvena[1] · Bincy John[1] · R. Anne Sarah Christinal[1] ·
M. C. Santhosh Kumar[2] · Sujay Chakravarty[3] · A. Leo Rajesh[1]

Abstract Thin films of quaternary chalcogenide Cu$_2$ZnSnS$_4$ (CZTS) were prepared due to its abundance and non-toxic nature by chemical spray pyrolysis technique with 2-methoxyethanol as solvent for the precursor solution that avoids the insoluble base by-products of zinc and tin. The solution was clear without precipitates as the solvent has higher viscosity compared to DI water which resulted in the successful deposition of smoother films. The structural, morphological, optical and electrical properties of the films at different temperatures 280, 300, 350 and 400 °C were investigated. The structural formation of kesterite Cu$_2$ZnSnS$_4$ was confirmed with a preferential (112) phase and with an intensed 334 cm^{-1} Raman frequency mode. Uniform film growth and crack-free surface was obtained at a temperature of 350 °C which was confirmed from morphological studies. The optical absorption showed a continuous absorption in the UV–Visible region and the obtained band gap for the films was in the range of 1.45–1.62 eV. The electrical study using Hall measurement proved the p-type conductivity of CZTS thin films which is pertinent for an absorber layer in thin film photovoltaic cell. A p–n junction was formed with TiO$_2$ and CZTS materials and the light and dark current response was studied.

1 Introduction

The modern cognizance of clean energy usage leads to the renovation of solar energy research which progresses to the state-of-the-art thin film solar cell technology. The thin film solar cell technology has been developing with different emergent materials. CdTe is a binary material with a latest efficiency of 16.5% and CuInGaSe$_2$ is a quaternary material with a newest maximum efficiency of >21.5% [1, 2]. Cu$_2$ZnSn(SSe)$_4$ and Cu$_2$ZnSnS$_4$ are also quaternary chalcogenide materials with the most recent efficiencies of 12.6 and 8.4% respectively [3, 4]. Among these materials Cu$_2$ZnSnS$_4$ (CZTS) attained a distinctive consideration because of its innoxious nature, less expensive and sufficient source availability aspects [5]. Moreover, CZTS is a p-type absorber layer in the photovoltaic cell with a direct optimum band gap of 1.45 eV and has an absorption coefficient of >10^4 cm^{-1} [6]. The UV-Vis region reaches maximum from the solar spectrum to Earth's surface and this material is suitable for absorbance in this region [7]. This material has a wide range of application in all the fields including antibacterial activity and biomedical application with a specific interest in photovoltaics [8, 9].

A number of deposition techniques were employed to prepare CZTS thin films for the fabrication of solar cell. Vacuum based techniques like pulsed laser deposition,[10] RF sputtering, [11] thermal evaporation, [12] and chemical methods such as chemical bath deposition, [13] spin coating, [14, 15] dip coating [16] and spray pyrolysis [17, 18] were used. Among these techniques spray pyrolysis is an inexpensive and wide surface area applicable technique.

✉ A. Leo Rajesh
aleorajesh@gmail.com

1 Department of Physics, St. Joseph's College (Autonomous), Tiruchirappalli, Tamilnadu 620002, India

2 Department of Physics, National Institute of Technology, Tiruchirappalli, Tamilnadu 620015, India

3 UGC-DAE Consortium for Scientific Research, Kalpakkam, Tamilnadu 603104, India

The CZTS thin films deposited using chemical spray pyrolysis technique are uniform and thick which is suitable for absorber layer in photovoltaic cell. Since both the method and the material are low-cost and high yield, it is of significant interest to the researchers. Various levels of optimizations like concentration variation, [19] precursor effect, [20] doping, [21] pH [22] etc. are already being done on this material using spray pyrolysis technique. The main drawback experienced in the spray technique for CZTS thin films is the precursor solution preparation. The instability in the precursor solution preparation leads to the precipitate formation which complicates the spraying of solution. In order to overcome this, the precursor solution is being prepared in different approaches like the use of different solvents methanol, hydrazine, ethanol/water, dimethyl sulfoxide, etc.[23–25] and the arrangement of mixing order of source materials [26] are done.

The novelty of this work stipulates the use of 2-methoxyethanol as solvent in precursor solution preparation for chemical spray pyrolysis deposition. The precursor sources chosen for this work is $CuCl_2$, $ZnCl_2$, $SnCl_2$ and thiourea. Among these elements $ZnCl_2$ and $SnCl_2$ are not easily soluble in water and forms insoluble base materials in the solution. In order to avoid this problem the solvent 2-methoxyethanol is used which has a boiling point of 124–125 °C and is mostly used in sol–gel preparation due to its optimum viscosity. The effect of solvent is studied at different temperatures 280, 300, 350 and 400 °C and the precursor solutions were free from precipitates which lead to the easy and repeatable preparation of solution on necessary situations.

2 Experimental Preparation

2.1 Materials

The precursor materials for Copper, Zinc, Tin and Sulfur elements were Copper(II) chloride dihydrate ($CuCl_2 \cdot 2H_2O$) 10 mM, Zinc chloride ($ZnCl_2 \cdot 2H_2O$) 5 mM, Tin(II) chloride dihydrate ($SnCl_2 \cdot 2H_2O$) 5 mM and Thiourea (CH_4N_2S) 40 mM respectively. Titanium(IV) isopropoxide was used as precursor for Titanium. 2-methoxyethanol was used as solvent for CZTS preparation and isopropyl alcohol was used as solvent for TiO_2 preparation. The precursors were purchased in Merck grade and used as purchased without any further purification.

2.2 Preparation of Precursor Solution and Deposition of Thin Films

A precursor solution has to be prepared without precipitates in order to deposit CZTS thin films using chemical spray pyrolysis technique. The solution was prepared by dissolving the above mentioned respective precursor materials in 80 ml of solvent. 2-methoxyethanol was used as the solvent in order to dissolve the precursor solution without any formation of precipitates. The solution was stirred for half an hour in the magnetic stirrer at room temperature and a colorless solution was obtained. The prepared solution was sprayed onto the preheated SLG substrates. The substrates were previously cleaned by sonicating in soap solution followed by HCl and finally with double distilled water and it was used immediately after washing. The pressure was fixed as 1.2 Kg cm^{-2} using compressed air as the carrier gas and the spray rate was maintained at 6 ml min^{-1}. The substrate to nozzle distance was approximately kept at 25 cm. The films were deposited continuously with 30 s spraying and 30 s decomposing process for eight times. The films were prepared at different substrate temperatures such as 280, 300, 350 and 400 °C. The film deposited at 250 °C did not spread uniformly due to less evaporation and pyrolysis effect at lower temperature and the films appeared as a solution sprinkled over the substrate. The samples were denoted as 280C, 300C, 350C and 400C for the films deposited at 280, 300, 350 and 400 °C respectively in the following discussions.

2.3 Characterization

The prepared films were characterized to confirm the structure and phase identification by using (Bruker D8 Discover) Glancing incidence X-Ray Diffractometer and (Renishaw inVia) Raman microscope at room temperature. The Bruker D8 Discover High resolution X-ray Diffractometer was used to study the GIXRD pattern of Cu_2ZnSnS_4 thin film at a scanning range of 15° to 70° and a step size of 0.04° with the $CuK_{\alpha1}$ source radiation (= 1.54051 Å). The Raman spectrum was recorded at room temperature using 785 nm near IR laser source wavelength.

The surface morphology and cross-section was studied using (Carl Zeiss) field emission scanning electron microscope with 10 kV extra-high tension (EHT) voltage. The optical properties of the CZTS thin films were studied to observe the absorption region and to acquire the band gap using (Jasco V670) UV–Visible-NIR spectrophotometer. The electrical properties of the prepared films were studied using (ECOPIA AMP 55) Hall Effect measurement system. The type of conductivity, carrier concentration, resistivity, mobility and Hall coefficient were all studied using this system. The photocurrent response was studied using keithley (source meter 2450) and Xenon lamp source.

3 Results and Discussion

3.1 Structural Analysis

Figure 1a gives the glancing incidence X-ray diffraction (GIXRD) pattern of CZTS thin films with prominent peaks at Bragg angle $2\theta = 28.5°$, $47.5°$ and $56.2°$ which agrees with the standard value for Kesterite tetragonal Cu_2ZnSnS_4 phase (JCPDS: 26–0575) with lattice plane orientation along (112), (220) and (312) direction respectively [27]. The CZTS thin films deposited at 280, 300 and 350 °C using 2-methoxyethanol solvent shows polycrystalline nature with a strong orientation along (112) phase. From the GIXRD pattern it is evident that the crystalline nature of the material deposited with solvent increases with increase in temperature and there is no significant change in the crystallite size with respect to the temperature. The 350 °C film contributes maximum intensed peaks showing good crystallinity.

(a)

(b)
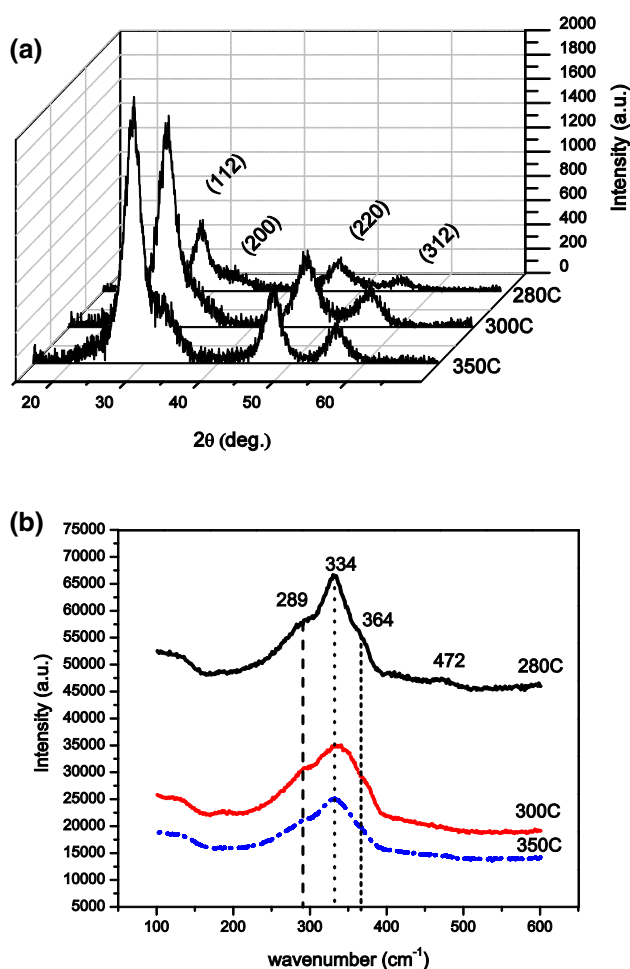
Fig. 1 a GIXRD pattern of CZTS thin films at different temperatures and **b** Raman spectrum of Cu_2ZnSnS_4 thin films

The crystallite size was calculated using the Debye–Scherrer's formula [28]

$$D = \frac{0.9\lambda}{\beta \cos\theta} \tag{1}$$

where D is the crystallite size, λ is the wavelength of the target $CuK\alpha_1(= 1.54051)$, β is the full-width half maximum value and θ is the position of respective Bragg peaks.

The crystallite size is in the range of 3–5 nm which shows broad diffraction peaks in Fig. 1a. The condensed crystallite size is resulted from the super saturation of precursors in the solvent. The 350 °C was reported as optimized temperature for the aqueous CZTS thin films as per the literature [29].

The phase confirmation of Cu_2ZnSnS_4 thin films is insufficient with XRD patterns alone since other structures like ZnS and Cu_2SnS_3 also show similar XRD pattern [30]. In order to confirm the crystal structure and the phase purity, Raman spectrum details are necessary for Cu_2ZnSnS_4 thin films. Figure 1b gives the room temperature Raman spectrum of Cu_2ZnSnS_4 thin films. The utilization of higher excitation wavelength like 785 nm would be helpful in fluorescence suppression and the detection of various secondary phases and oxides [31]. The Raman spectra were covered in the range from 100 to 600 cm^{-1}.

The broad and intensed mode located at 334 cm^{-1} indicates the formation of Cu_2ZnSnS_4 phase and a shoulder at 289 cm^{-1} also shows the presence of Cu_2ZnSnS_4 phase [32–34]. The prominent peaks 334 and 289 cm^{-1} arises from A1 vibration mode in which only Sulphur S^{2-} anions are involved whereas the weak mode at 367 cm^{-1} corresponds to B1 vibrational mode with cation moving in the z-direction [35–37]. The presence of 472 cm^{-1} [38] mode in 280 °C shows the Cu_2S impurity phase formation which was later missing in the films prepared at higher temperatures. This infers that the impurity phase formation reduces with increase in temperature.

3.2 Morphological Studies

Figure 2 shows the surface morphology and the cross-sectional FESEM images. There is a significant variation in the surface morphology of the films with respect to temperature. The surface morphology details explain that the film 350 °C acquire nano flakes structure and are uniform without cracks [39]. From Fig. 2c it is observed that at 350 °C temperature the film growth is uniform and for all other temperatures micro cracks are seen which show the discontinuity in the upper surface of the coating. Since CZTS is a polycrystalline material the grain boundaries are seen in the image. The inset shows cross-sectional image of the samples which is used to measure the thickness of thin film. The thickness of the samples is 548.8, 628.4, 767.7 and 891.5 nm for 280, 300, 350
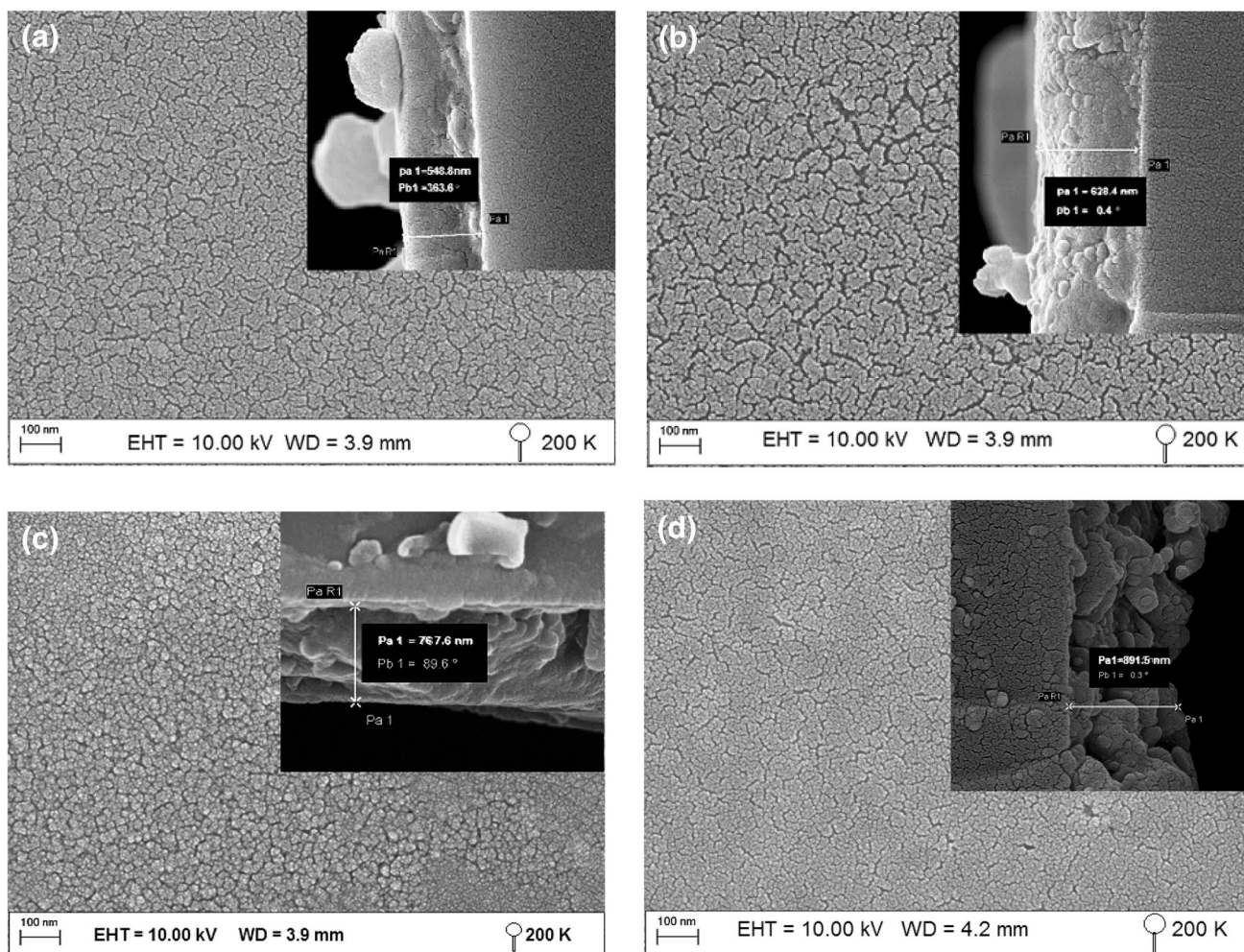
Fig. 2 FESEM morphology of **a** 280 °C **b** 300 °C **c** 350 °C **d** 400 °C and *inset* is the cross-section of each sample respectively

and 400 °C respectively. There is no agglomeration in the surface since there is no precipitate formation.

3.3 Optical Studies

Figure 3a shows the absorption spectra of Cu_2ZnSnS_4 thin films taken by UV–Visible spectrophotometer. The spectra show maximum absorption at 300–350 nm followed by a continuous absorption in the visible region and reduces down to the near IR region about 900 nm. The cut-off wavelength in the near IR region shows that the material is suitable for solar cell application. The optical band gap of the films was calculated using Tauc plot as shown in Fig. 3b. The direct band gap is obtained from the extrapolation of the linear part of the curve in the plot of hν in eV versus $(\alpha h\nu)^2$ in $(cm^{-1}\ eV)^2$. The optical band gap is calculated using the formula [40].

$$\alpha h\nu = A[h\nu - E_g]^n \tag{2}$$

where absorption coefficient, A is a constant, Eg is the band gap energy and n = ½ for direct allowed transitions.

The Tauc plot gives the direct band gap of the samples which is suitable for absorber layer. The band gap is obtained as 1.62, 1.60, 1.45 and 1.54 eV for 280C, 300C, 350C and 400C respectively. The optimum band gap applicable for absorber layer in photovoltaic cell was obtained for 350C film. The band gap was reducing from 280C to 350C, reached the optimum value at 350C and again increases to higher value at 400C [15]. As the thickness increases the color of the film improves from dark brown to black color [41] and it is seen that the absorption edge is in the near IR region. The absorbance also improves at higher temperature due to the thickness of the film. The absorption coefficient of the films is found to be $10^4\ cm^{-1}$ which is suitable for photovoltaic application.

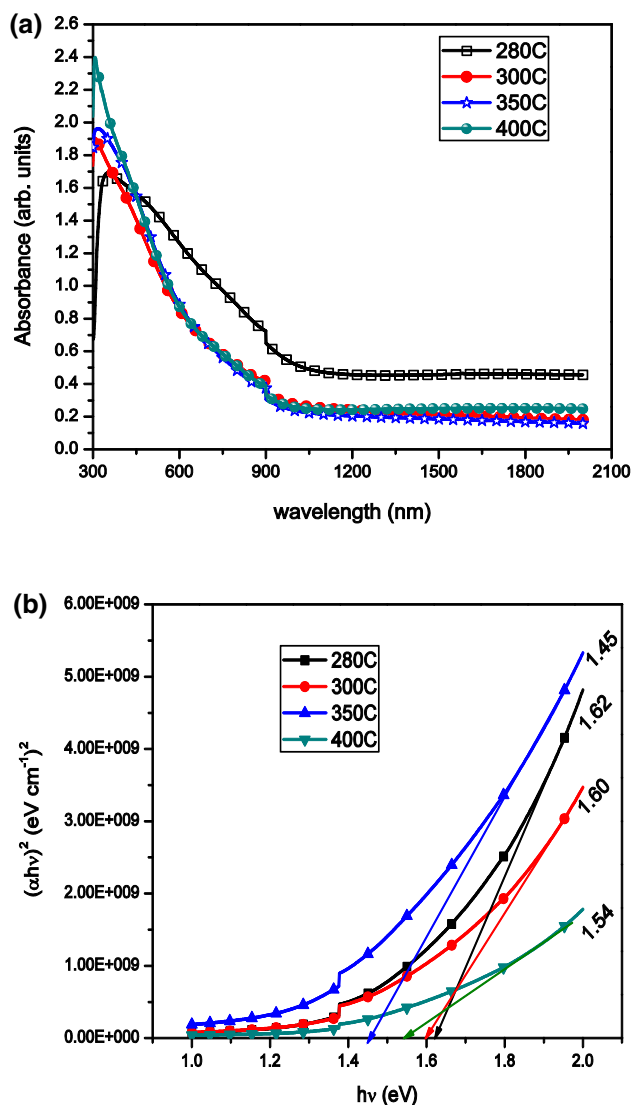**Table 1** Carrier concentration, mobility, resistivity and Hall co-efficient of CZTS thin films

Sample (ºC)	Carrier concentration (cm^{-3})	Mobility (cm^2 V^{-1} s^{-1})	Resistivity (Ω cm)	Hall coefficient (cm^3 C^{-1})
280	3.24×10^{13}	180	1070	193,000
300	6.92×10^{14}	4.60	1960	9020
350	1.25×10^{15}	17.1	292	4980
400	4.53×10^{17}	1.95	7.08	13.8

of CZTS thin films. The variation in mobility, carrier concentration and Hall coefficient with temperature is shown in Fig. 4. It shows that mobility and Hall coefficient are inversely proportional to carrier concentration.

The photocurrent response of the device was studied and is shown in Fig. 5. The heterojunction FTO/TiO$_2$/CZTS/Ag was formed and studied. The response shows increase in current value for increase in temperature. It showed a maximum current response of 10 mA for 350 °C film which is shown in Fig. 5c. The Fig. 5a–d shows the light (l) and dark (d) current response.

4 Conclusion

The spray pyrolysed CZTS thin films were deposited without precipitates using 2-methoxyethanol solvent. The effect of solvent at different substrate temperatures revealed significant difference in the crystalline nature, surface morphology, optical absorption, band gap energy and electrical parameters. The carrier concentration and mobility had increased with temperature and all the films showed p-type conductivity. The photocurrent response also showed maximum current value for 350 °C. At 350 °C the film obtained

Fig. 3 **a** Absorption spectrum of Cu$_2$ZnSnS$_4$ thin films **b** Tauc plot

3.4 Electrical Studies

Hall measurement for the CZTS thin films was performed by applying 0.59 T magnetic field at room temperature and the contact was made with silver paste. All the films showed p-type conductivity which is pertinent for photovoltaic application. The samples show low resistivity at higher deposition temperature which indicates that the resistance decreases with increase in deposition temperature [42]. The carrier concentration, mobility, resistivity and Hall coefficient values are listed in Table 1. The carrier concentration increases with increase in temperature from 10^{13} to 10^{17} cm^{-3}, whereas the resistivity and mobility decreases with increase in temperature from 1070 to 7.08 Ω cm and 180 to 1.95 cm^2 V^{-1} s^{-1} respectively [15, 43]. The positive value of Hall coefficient denotes the p-type conductivity
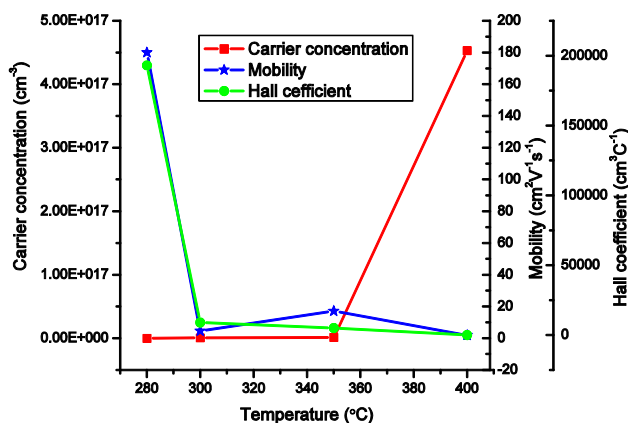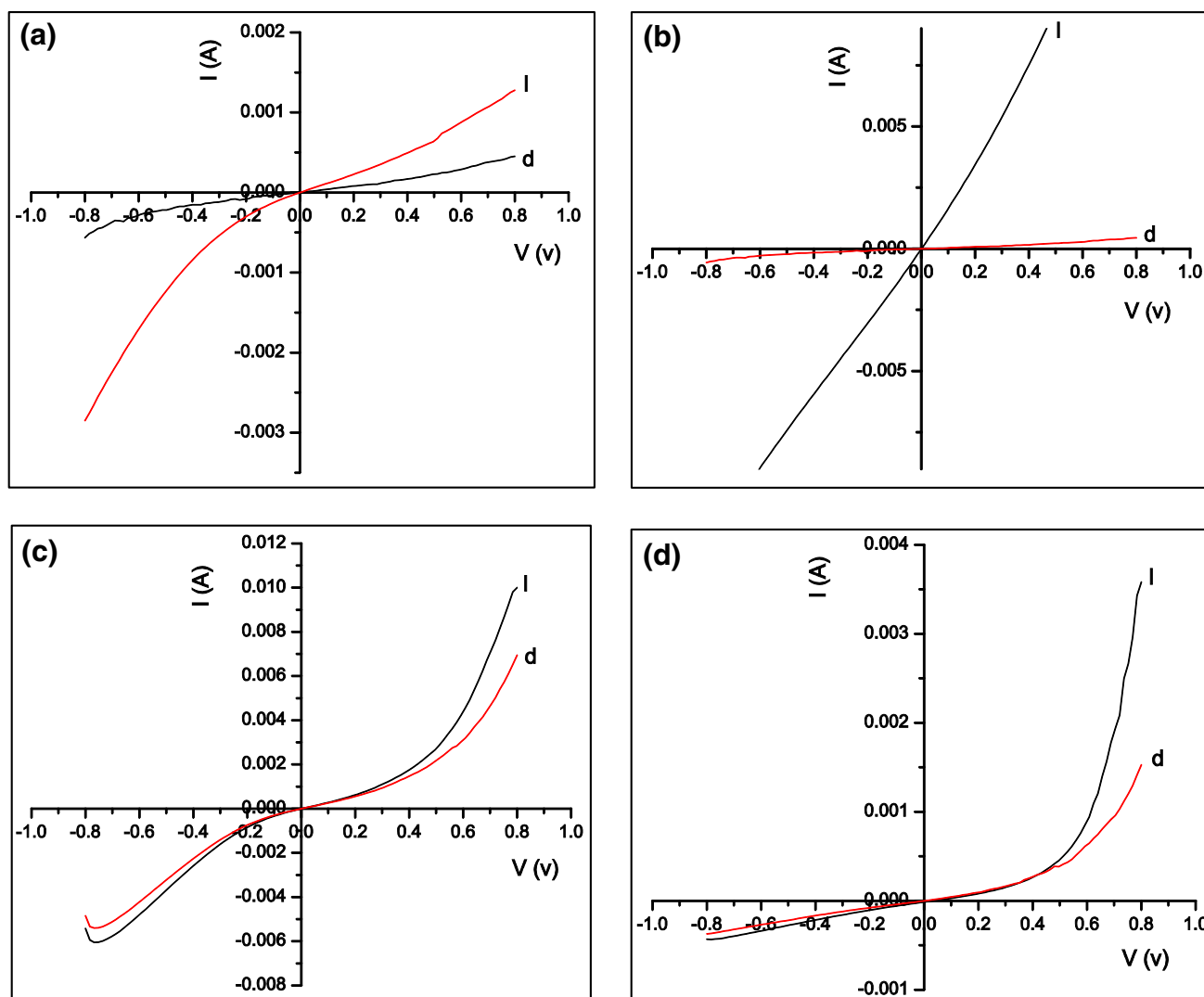

Fig. 4 Carrier concentration, mobility and Hall coefficient variation of CZTS films at different substrate temperatures

Fig. 5 Photocurrent response of **a** 280 °C **b** 300 °C **c** 350 °C and **d** 400 °C

optimum properties with 1.45 eV band gap which is suitable for absorber layer in thin film solar cells.

References

1. H.P. Mahabaduge, W.L. Rance, J.M. Burst et al., Appl. Phys. Lett. **106**, 13350–13351 (2015)
2. P. Jackson, D. Hariskos, R. Wuerz et al., Phys. Status Solidi **9**, 28 (2015)
3. W. Wang, T. Mark Winkler, O. Gunawan et al., Adv. Energy Mater. **4**, 1 (2014)
4. M.A. Green, K. Emery, Y. Hishikawa, W. Warta, D.E. Dunlop, Prog. Photovolt **23**, 1 (2015)
5. N. Nakayama, K. Ito, Appl. Surf. Sci. **92**, 171 (1996)
6. K. Ito, T. Nakazawa, Jpn. J. Appl. Phys. **27**, 2094 (1988)
7. E.H. Sargent, Nat. Photon. **3**, 325 (2009)
8. R. Saravana Kumar, S. Maddirevula, M. Easwaran, S.H.S. Dananjaya, M.-D. Kim, RSC Adv. **5**, 106400 (2015)
9. A. Angelova, B. Angelov, R. Mutafchieva, S. Lesieur, J. Inorg. Organomet. Polym. **25**, 214 (2015)
10. S.A. Vanalakar, G.L. Agawane, S.W. Shin et al., J. Alloy Compd. **619**, 109 (2015)
11. J.-S. Soel, S.-Y. Lee, J.-C. Lee, H.-D. Nam, K.-H. Kim, Sol. Energy Mater. Sol. Cells **75**, 155 (2003)
12. K. Wang, O. Gunawan, T. Torodov, B. Shin, S.J. Chey et al. Appl. Phy. Lett. **97**, 143508 (2010)
13. A. Wangperawong, J.S. King, S.M. Herron, B.P. Tran, K. Pangan-Okimoto, S.F. Bent, Thin Solid Films **519**, 2488 (2011)
14. M.Y. Yeh, C.C. Lee, D.S. Wuu, J. Sol-Gel Sci. Technol. **52**, 65 (2009)
15. S.K. Swami, A. Kumar, V. Dutta, Energy Procedia, **33**, 198 (2013)

16. G. Rajesh, N. Muthukumarasamy, E.P. Subramanian, S. Agilan, D. Velauthapillai. J. Sol-Gel Sci. Technol. **66**, 488 (2013)
17. D. Song, W. Kim, K. Mahmood et al., J. Alloy Compd. **567**, 89 (2013)
18. S. Thiruvenkadam, D. Jovina, A.L. Rajesh, Sol. Energy **106**, 166 (2014)
19. Y.B. Kishore Kumar, P. Uday Bhaskar, G. Suresh Babu, V. Sundara Raja, Phys. Status Solidi A **207**, 149 (2010)
20. V.G. Rajeshmon, C. Sudha Kartha, K.P. Vijaya Kumar, C. Sanjeeviraja, T. Abe, Y. Kashiwaba, Sol. Energy **85**, 249 (2011)
21. K. Prashant Saraswat, L. Michael Free, J. Mater. Sci. **50**, 1613 (2015)
22. Y.B. Kishore Kumar, G. Suresh Babu, P. Uday Baskar, V. Sundara Raja, Phys. Status Solidi A **206**, 1525 (2015)
23. K. Woo, Y. Kim, J. Moon, Energy Environ. Sci. **5**, 5340 (2012)
24. W. Daranfed, M.S. Aida, N. Attaf, J. Bougdira, H. Rinnert, J. Alloy Compd. **542**, 22 (2012)
25. W. Ki, W.H. Hillhouse, Adv. Energy Mater. **1**, 732 (2011)
26. T.H. Nguyen, W. Septina, S. Fujikawa et al., RSC Adv. **5**, 77565 (2015)
27. H.T. Kim, D. Kim, C. Park, Mol. Cryst. Liq. Cryst. **564**, 155 (2012)
28. M. Valdes, G. Santoro, M. Vazquez, J. Alloy Compd. **585**, 776 (2014)
29. S.K. Swami, N. Chaturvedi, A. Kumar, V. Dutta, Sol. Energy **122**, 508 (2015)
30. G.L. Agawane, S.W. Shin, S.A. Vanalakar et al., J. Mater. Sci. **26**, 1900 (2015)
31. O. Awadallah, Z. Cheng J. Photovolt. **6**, 764 (2016)
32. Z. Seboui, A. Gassoumi, Y. Cuminal, N. Kamoun Turki, J. Renew. Sustain. Energy **7**, 011203 (2015).
33. Y. Liu, J. Xu, Z. Ni, G. Fang, W. Tao, J. Alloy Compd. **630**, 23 (2015)
34. G. Gurieva, M. Guc, L.I. Bruk et al., Phys. Status Solidi C **10**, 1082 (2013)
35. R. Moreno, E.A. Ramirez, G. Gordillo Guzman, JPCS **687**, 012041 (2016)
36. E. Ramirez, A. A. Ramirez, M. F. Hurtado, G. Gordillo, IEEE (2015)
37. L.I. Bruc, M. Guc, M. Rusu, D.A. Sherban et al., in *Proceedings of 27th European Photovoltaic Solar Energy Conference and Exhibition*, 2763 (2012)
38. Z. Seboui, Y. Cuminal, N. Kamoun-Turki, J. Renew. Sustain. Energy **5**, 023113 (2013)
39. K.G. Deepa, N. Jampana, J. Anal. Appl. Pyrolysis **117**, 141 (2016)
40. S. Yazici, M. Olgar, F. G. Akca et al., Thin Solid Films **589**, 563 (2015)
41. N.M. Shinde, R.J. Deokate, C.D. Lokhande, J. Anal. Appl. Pyrolysis **100**, 12 (2013)
42. M.Z. Ansari, N. Khare, J. Phys. D **47**, 185101, (2014)
43. M. Adelifard Appl. Phys. A **121**, 95 (2015)